Int. J. Heat Mass Transfer. Vol. 32, No. 5, pp. 843–854, 1989
Printed in Great Britain

0017–9310/89 $3.00+0.00

Photophoresis of aerosol particles in the free molecular and slip-flow regimes

D. W. MACKOWSKI

Department of Chemical Engineering, High Temperature Chemical Reaction Engineering Laboratory, Yale University, New Haven, CT 06520-2159, U.S.A.

(*Received* 30 *May* 1988 *and in final form* 4 *October* 1988)

Abstract—An analysis of the photophoretic force and velocity on aerosol particles in both the free molecular and slip-flow regimes is presented. Under the assumption of unpolarized incident radiation, absorption of radiation with the particle is formulated from Lorenz/Mie theory. For both the free molecular and slip-flow regimes, the functional dependence of the photophoretic velocity upon the radiative size parameter and complex index of refraction is given by the photophoretic asymmetry factor J_1. An exact infinite-series expression for J_1 is derived which allows for rapid calculation of photophoretic behavior. Numerical results indicate that photophoresis can be a significant transport mechanism for micrometer-sized particulates in high radiative transfer combustion environments.

1. INTRODUCTION

THE IDENTIFICATION and analysis of small-particle transport mechanisms in combustion environments is an essential element to the accurate prediction of particulate deposition rates. Thermophoresis and inertial impaction are known to be important mechanisms and have been investigated extensively [1]. Less well known is the role of photophoretic particulate transport. Photophoresis is similar to thermophoresis in that particle motion is driven by a temperature gradient. In thermophoresis, the temperature gradient exists in the surrounding gas, whereas in photophoresis, the temperature gradient is on the particle surface and arises from the non-uniform absorption of radiant energy within the particle. Considering that radiative transfer can account for around 95% of the total heat flux in pulverized-coal (PC) furnaces [2], the 'driving force' for photophoresis in combustion environments can be significantly greater than that for thermophoresis. Because of this, an analysis of photophoresis in thermal radiation situations is certainly warranted.

Several theoretical investigations have attempted to quantify the photophoretic force F_p and velocity V_p of a particle. For particles in the free molecular limit (FML) regime, i.e. $Kn = l/a \gg 1$, where Kn is the Knudsen number, l the mean-free-path of the gas molecules and a the particle radius, solutions have been presented by Hidy and Brock [3], Tong [4], Ahktaruzzaman and Lin [5], and Sitarski and Kerker [6]. Reed [7] considered photophoresis in the slip-flow ($Kn < 1$) regime, and Yalamov *et al.* [8] examined the continuum ($Kn \ll 0$) situation.

An important difference among the above works is the manner in which absorption of radiation was formulated in the conduction equation for the particle temperature distribution. In refs. [3, 4, 7], it was assumed that the radiation incident upon the particle was absorbed entirely on the particle surface. Radiative energy transport to the particle was thus formulated as a boundary condition in the conduction equation. Such an approach is not physically realistic for micrometer-sized aerosol particles exposed to thermal radiation. For such situations, where the particle radii is comparable to the radiation wavelength λ, radiation absorption will be distributed throughout the particulate volume. Indeed, under certain conditions the radiant energy can be 'focused' into the back (non-illuminated) side of the particle, resulting in a higher temperature at this surface than the illuminated side and a corresponding particle motion towards the radiation source (negative photophoresis). Consequently, to accurately predict F_p and V_p it is necessary to formulate radiant energy transport to the particle through a source function in the conduction equation.

In general, the distribution of radiant absorption within a homogeneous sphere can be obtained from Lorenz/Mie theory as a function of the radiative size parameter $x = 2\pi a/\lambda$ and the complex refractive index $m = n + i\kappa$ [9]. This theory was adopted in the analytical, closed-form solutions for F_p given in refs. [5, 8]. Numerical evaluation of the solutions is not a trivial task, due to the complexities of Lorenz/Mie theory. At present, calculations of F_p for general x and m are limited to those presented by Pluchino [10] for the continuum theory of ref. [8], and Kerker and Cooke [11] for the FML theory of ref. [5]. The FML analysis of Sitarski and Kerker [6] also incorporated the Lorenz/Mie source function, but involved a numerical, Monte-Carlo technique in the solution of the energy and momentum equations.

The results of ref. [10] were found to agree well with measurements of F_p performed by Arnold and Lewittes [12]. Accurate experimental validations of

NOMENCLATURE

a	sphere radius
A_1, A_2, A_3	coefficients in Millikan drag formula, equation (31)
B	dimensionless radiative intensity distribution function
c_m, c_s, c_t	momentum exchange, thermal slip, and temperature jump coefficients
c_n, d_n	internal electric field coefficients
c_p	specific heat of fluid
$\mathbf{E}$	electric field amplitude vector
F	force
g	dimensionless heat source distribution function
g_n	function of ζ defined by equation (7)
G_n	function of ζ defined by equation (10)
H_m	defined by equation (35)
I	radiant intensity
J_1	photophoretic asymmetry factor
k	thermal conductivity
Kn	Knudsen number, l/a
l	gas molecule mean-free-path
Le	Lewis number
m	refractive index, $n+i\kappa$
n	real part of refractive index
P	gas pressure
P_n	Legendre polynomial
q_R	radiative heat flux
Q	heat generation through radiation absorption
Q_{abs}	absorption efficiency of particle
r	radial position
R	specific gas constant
R_n, S_n	functions of m, x given in equations (59) and (61)
T	temperature
$\mathbf{v}$	fluid velocity vector
V	particle velocity
x	radiative size parameter.

Greek symbols

α	thermal accommodation coefficient
$\alpha_p D$	photophoretic diffusivity
ζ	dimensionless radial position
η	dynamic viscosity
κ	imaginary part of refractive index
λ	wavelength
μ	$\cos\theta$
π_n, τ_n	angular scattering functions
ρ	density or dimensionless radiative radial coordinate
τ	thermal response time
ϕ, θ	azimuth and polar coordinates
ψ_n	Ricatti–Bessel function.

Subscripts

g	gas phase
p	photophoretic
r, θ, ϕ	spherical coordinate system component
s	solid phase
T	thermophoretic
0	ambient
λ	spectral component.

Superscripts

*	complex conjugate
¯	normalized or wavelength averaged.

the FML predictions for F_p have currently not been performed.

The numerical complexity involved in evaluation of F_p and V_p from the above Lorenz/Mie-based theories limit their applicability to a wide range of problems. For instance, calculation of V_p for a broad-band source of radiation, e.g. thermal radiation, would add another obstacle to an already difficult task. Developed here are theories for photophoresis in both the free molecule and slip-flow region which incorporate the Lorenz/Mie source yet allow for a relatively simple calculation, in that determination of V_p involves a computation equivalent to determination of the radiative cross sections of the particle. A central assumption in the theory is that the incident radiation is unpolarized, which results in a heat generation function that is independent of azimuth angle. Such would be the case for thermal radiation. This assumption was adopted by Yalamov *et al.* [8]; indeed, the theory presented here represents a velocity-slip corrected solution to the continuum theory of ref. [8]. The free molecule theory of Ahktaruzzaman and Lin [5] considers the full three-dimensional problem, yet the theory presented here is shown to qualitatively agree with this work.

The analysis begins with the general solution to the conduction equation for a sphere, which is central to both the slip-flow and free molecule regimes. Theories are then developed for these two regimes. A closed-form solution for the radiative parameter governing F_p and V_p as a function of x and m is presented, and comparisons are made with previous theories and experiments. Finally, the role of photophoresis in combustion environments is discussed.

2. SOLUTION OF THE CONDUCTION EQUATION

Solutions to the spherical geometry conduction equation for non-uniform heat generation have been

presented for both three- [5] and two-dimensional [8] cases. In general, the rotation of the particle with respect to the incident radiation field will result in a time-dependent problem. The thermal response time of the particle $\tau_s = a^2/4\alpha_s$, where α_s is particle thermal diffusivity, will generally be much smaller than the time associated with diffusional particle rotation [13]. Particle rotation will also result from rotation of the surrounding fluid, which, in the turbulent flows associated with large-scale PC combustors, can be significant. However, as is the case with thermophoresis, the effect of photophoresis upon particulate deposition will be of greatest significance in the transport of particulates across the viscous sublayer [1, 14]. In this region τ_s will typically be much smaller than the fluid rotation time. Consequently, a quasi-steady analysis can be used in which the coordinate system of the particle is fixed relative to the incident radiation direction.

It is also assumed that the particle is nonvolatile. Vaporization of volatile components from the particle surface will, generally, influence the overall photophoretic force, and such considerations have been investigated in refs. [6, 8]. It has been noted, however, that the 'jetting' action of a devolatilizing coal particle can result in rotation rates of the order of 1000 s^{-1}, which would bring into question a quasi-steady analysis of the conduction equation [15]. Particles in the boundary layer, which again are of prime interest in consideration of deposition rates, can be reasonably expected to be completely devolatilized.

For the problem at hand, the radiation is assumed to propagate in the positive z-direction. In spherical coordinates and for azimuthal symmetry, conservation of energy is expressed as

$$\nabla^2 T_s = \frac{1}{r^2}\frac{\partial}{\partial r}\left(r^2\frac{\partial T_s}{\partial r}\right) + \frac{1}{r^2}\frac{\partial}{\partial \mu}\left[(1-\mu^2)\frac{\partial T_s}{\partial \mu}\right] = -\frac{Q(r,\mu)}{k_s} \quad (1)$$

where T_s is the particle temperature, $\mu = \cos\theta$, k_s the thermal conductivity, and $Q(r,\mu)$ the volumetric energy generation rate resulting from local radiation absorption. An implicit assumption in equation (1) is that the radiative energy transfer due to thermal emission within the particle is insignificant compared to conduction heat transfer. Although thermal emission may become important at combustion temperatures, full coupling of radiative transfer and conduction equations is beyond the scope of the present analysis.

The radiant-absorption heat generation function Q can be related to the electric field $\mathbf{E}$ with the particle [9]. For monochromatic incident radiation, Q is given by

$$Q(r,\mu) = \frac{4\pi n\kappa I_\lambda}{\lambda}\frac{|\mathbf{E}(r,\mu)|^2}{|\mathbf{E}_0|^2} = \frac{4\pi n\kappa I_\lambda}{\lambda}B(r,\mu) \quad (2)$$

where n and κ are the real and imaginary parts of the refractive index m, I_λ the intensity of the incident radiation, $\mathbf{E}_0$ the incident electric field strength, and $B(r,\mu)$ the dimensionless electric field distribution function. Defining non-dimensional quantities $\bar{T} = (T_s - T_0)/T_0$, $\zeta = r/a$, and $g = a^2Q/k_sT_0$, where T_0 is the mean temperature of the surrounding fluid, equation (1) becomes

$$\frac{\partial}{\partial\zeta}\left(\zeta^2\frac{\partial\bar{T}}{\partial\zeta}\right) + \frac{\partial}{\partial\mu}\left[(1-\mu^2)\frac{\partial\bar{T}}{\partial\mu}\right] = -\zeta^2 g(\zeta,\mu). \quad (3)$$

The solution to equation (3) is given as the sum of the homogeneous and particular solutions, denoted by T_1 and T_2, respectively. The homogeneous solution that is valid at the origin is

$$T_1 = \sum_{n=0}^{\infty} A_n\zeta^n P_n(\mu) \quad (4)$$

where A_n are undetermined coefficients and $P_n(\mu)$ the Legendre polynomial. The particular solution can be obtained from a transformation of equation (3) into an ordinary differential equation. Multiplying equation (3) through by $(n+1/2)^{1/2}P_n(\mu)\,d\mu$, integrating from -1 to 1, and utilizing Legendre's equation yields

$$\frac{d}{d\zeta}\left(\zeta^2\frac{du_n}{dr}\right) - n(n+1)u_n = -g_n \quad (5)$$

where

$$u_n(\zeta) = \left(\frac{2n+1}{2}\right)^{1/2}\int_{-1}^{1} T_2(\zeta,\mu)P_n(\mu)\,d\mu \quad (6)$$

and

$$g_n(\zeta) = \left(\frac{2n+1}{2}\right)^{1/2}\zeta^2\int_{-1}^{1} g(\zeta,\mu)P_n(\mu)\,d\mu. \quad (7)$$

The solution to equation (5) is obtained from variation of parameters, to yield

$$u_n(\zeta) = \frac{\zeta^{-(n+1)}}{2n+1}\int_0^{\zeta} t^n g_n(t)\,dt + \frac{\zeta^n}{2n+1}\int_{\zeta}^{1} t^{-(n+1)}g_n(t)\,dt. \quad (8)$$

Thus, the solution to equation (3) is

$$\bar{T} = \sum_{n=0}^{\infty}(A_n\zeta^n + G_n(\zeta))P_n(\mu) \quad (9)$$

where

$$G_n(\zeta) = \frac{1}{2}\left(\zeta^n\int_{\zeta}^{1} t^{1-n}\int_{-1}^{1} g(t,\mu)P_n(\mu)\,d\mu\,dt + \zeta^{-(n+1)}\int_0^{\zeta} t^{n+2}\int_{-1}^{1} g(t,\mu)P_n(\mu)\,d\mu\,dt\right). \quad (10)$$

3. SLIP-FLOW REGIME PHOTOPHORESIS

For particles in the size range $Kn = l/a < 1$, where Kn is the Knudsen number and l the mean-free-path of the gas molecules, the analysis of photophoresis can be approached from a continuum viewpoint with the addition of slip-corrected boundary conditions. This approach was adopted in the slip-flow regime photophoresis analysis of Reed [7], although the exact nature of radiant absorption within the particle was not considered. It would not be expected that the functional dependence of F_p upon Kn would be affected by the particular model taken for radiant absorption; indeed, Arnold *et al.* [16] have indicated that the slip-correction factor for the continuum-theory expression of Yalamov *et al.* [8] is precisely that obtained in ref. [7]. For the sake of completeness, however, the slip-flow regime analysis for F_p and V_p is presented below.

Assuming $Re \ll 1$, where Re is the Reynolds number of the sphere, the governing differential equations for the problem are

$$\nabla^2 T_g = \frac{\rho_g c_p}{k_g}\left(\frac{v_\theta}{r}\frac{\partial T_g}{\partial \theta} + v_r \frac{\partial T_g}{\partial r}\right) \tag{11}$$

$$\nabla^2 T_s = -\frac{Q(r,\mu)}{k_s} \tag{12}$$

$$\nabla^2 \mathbf{v} = \frac{1}{\eta}\nabla P \tag{13}$$

$$\nabla \cdot \mathbf{v} = 0. \tag{14}$$

The boundary conditions for the above are

$$T_g - T_s = c_t l \frac{\partial T_g}{\partial r}, \quad r = a \tag{15}$$

$$k_g \frac{\partial T_g}{\partial r} = k_s \frac{\partial T_s}{\partial r}, \quad r = a \tag{16}$$

$$T_g = T_0, \quad r \to \infty \tag{17}$$

$$v_r = 0, \quad r = a \tag{18}$$

$$v_\theta = c_m l\left[r\frac{\partial}{\partial r}\left(\frac{v_\theta}{r}\right) + \frac{1}{r}\frac{\partial v_r}{\partial \theta}\right] + \frac{c_s \eta}{\rho_g T_0 a}\frac{\partial T_g}{\partial \theta}, \quad r = a \tag{19}$$

$$\mathbf{v} = V_0, \quad r \to \infty. \tag{20}$$

In the above, T_g, η, ρ_g and c_p are the temperature, viscosity, density, and specific heat of the gas. Equation (15) is the temperature-jump condition, in which the coefficient c_t is of the order of unity. Omitted in equation (16) is radiative heat transfer from the particle, which is here assumed negligible. Equation (19) gives the tangential velocity slip at the particle surface, where c_m and c_s are the momentum exchange and thermal slip coefficients. It is precisely the tangential velocity slip which results in the photophoretic force for this size regime. Values of the coefficients c_t, c_m, and c_s are obtained from kinetic theory as 2.18, 1.14, and 1.17, respectively [17].

An exact solution to the system of equations (11)–(20) has not been developed. Brock [18] utilized a perturbation technique to develop an approximate solution for the slip-flow thermophoresis problem, in that T_g, T_s, v_r, and v_θ were expanded in terms of the dimensional parameter $\beta = c_s\eta/\rho_g T_0$. On the first-order approximation his analysis is equivalent to neglecting the convection term (right-hand side) in equation (11). The contribution to the thermophoretic force by higher-order approximations was found to be negligible.

The same approach is utilized here. With the convection term removed from equation (11), the general solution is

$$\bar{T}_g \equiv \frac{T_g - T_0}{T_0} = \sum_{n=0}^{\infty} D_n \zeta^{-(1+n)} P_n(\mu). \tag{21}$$

Utilizing equations (9), (15), and (16), the coefficients D_n are solved as

$$D_n = \frac{G_n'(1) - nG_n(1)}{n + (n+1)k_g/k_s + n(n+1)c_t l/a} \tag{22}$$

where the prime denotes differentiation with respect to the argument. The general solutions to hydrodynamic equations (13) and (14) are [8]

$$v_r = \sum_{n=1}^{\infty} f_{rn}(\zeta) P_n(\mu) \tag{23}$$

$$v_\theta = \sum_{n=1}^{\infty} f_{\theta n}(\zeta) P_n^{(1)}(\mu) \tag{24}$$

$$P = \sum_{n=1}^{\infty} f_{pn}(\zeta) P_n(\mu) \tag{25}$$

where f_{rn}, $f_{\theta n}$, and f_{pn} are undetermined functions of ζ alone and $P_n^{(1)}(\mu)$ is the associated Legendre function. When the corresponding stress tensor obtained from equations (23)–(25) is integrated over the sphere surface, all terms except $n = 1$ vanish due to the orthogonality of the Legendre functions. Consequently, the problem effectively reduces to the case of Stokes flow past a sphere. For this situation [19]

$$v_r = V_0\left(1 - \frac{2c_1}{\zeta} + \frac{2c_2}{\zeta^3}\right)\cos\theta \tag{26}$$

$$v_\theta = -V_0\left(1 - \frac{c_1}{\zeta} - \frac{c_2}{\zeta^3}\right)\sin\theta \tag{27}$$

where c_1 and c_2 are undetermined coefficients. Using boundary conditions (18)–(20), one obtains

$$c_1 = \frac{3}{4}\frac{(1 + 2c_m l/a)}{(1 + 3c_m l/a)} - \frac{1}{2}\frac{c_s \eta [G_1'(1) - G_1(1)]}{V_0 \rho_g a (1 + 3c_m l/a)(1 + 2c_t l/a + 2k_g/k_s)}. \tag{28}$$

The force acting upon the particle can now be obtained from the relation $F = 8\pi a \eta V_0 c_1$ [19]. The first term in equation (28) will yield the Basset slip-

flow correction to Stokes drag, and the second term represents the photophoretic force contribution. Using equations (10) and (2) in the term $G_1'(1) - G_1(1)$, this force is

$$F_p = -\frac{4\pi c_s \eta^2 I_\lambda a J_1}{\rho_g k_s T_0} \times [(1+3c_m l/a)(1+2c_t l/a+2k_g/k_s)]^{-1} \quad (29)$$

where

$$J_1(x,m) = 3n\kappa x \int_0^1 \int_{-1}^1 B(t,\mu) t^3 \mu \, d\mu \, dt. \quad (30)$$

As mentioned previously, Reed [7] considered the case where radiation is absorbed entirely on the illuminated particle surface. Such a condition would correspond, in the analysis developed here, to a source function Q proportional to $\delta(\zeta-1)\mu$ on the illuminated side and equal to zero on the dark side, where δ is the delta function. For this situation it can be readily shown that $J_1 = -0.5Q_{abs}$, where Q_{abs} is the absorption efficiency of the particle, and equation (29) will become equal to the expression for F_p developed by Reed [7]. For the case where l/a and k_g/k_s both equal zero, equation (29) also corresponds exactly to the non-volatile particle solution given by Yalamov *et al.* [8]. Evaluation of the photophoretic asymmetry factor J_1 is discussed in Section 5.

The photophoretic velocity V_p is obtained by equation F_p to the local aerodynamic drag on the particle. The Millikan drag formula is more accurate than the Basset formula for near-unity Knudsen numbers, and is expressed as

$$F_d = \frac{6\pi\eta V_p a}{1+l/a(C_1+C_2 e^{-C_3 a/l})} \quad (31)$$

where $C_1 = 1.20$, $C_2 = 0.41$, and $C_3 = 0.88$ [17]. The expression for V_p in the slip-flow regime is thus given by

$$V_p = -\frac{2c_s \eta I_\lambda J_1}{3\rho_g k_s T_0} \frac{1+l/a(C_1+C_2 e^{-C_3 a/l})}{(1+3c_m l/a)(1+2c_t l/a+2k_g/k_s)}. \quad (32)$$

The sign convention on V_p is selected so that displacement in the direction of radiation propagation is considered positive.

4. FREE MOLECULAR REGIME PHOTOPHORESIS

For the situation where the particle radius is much smaller than the mean-free-path of the surrounding gas molecules, the photophoretic force on the particle can be obtained from consideration of the molecular momentum transfer to and from the particle surface. The analysis presented here closely follows that developed by Talbot *et al.* [17] for free molecular limit thermophoresis. In the following, the definition adopted for l is

$$l = 2\eta(\pi/8RT_0)^{1/2}/\rho_g$$

where R is the gas constant of the surrounding fluid, and the thermal conductivity of the gas is taken to be the translational component given by

$$k_g = \frac{15}{4}\eta R.$$

The incoming molecules are assumed to be distributed in velocity according to a Maxwellian distribution function evaluated at the ambient gas temperature T_0. All molecules are assumed to be reflected diffusely, which implies complete momentum accommodation. Complete thermal accommodation is not assumed, and the thermal accommodation coefficient α is defined as the ratio of the net molecular kinetic energy transfer to the particle to that if all reflected molecules were characterized by a Maxwellian distribution evaluated at the actual local surface temperature.

In general, the boundary condition for the energy equation and the momentum equation will have a non-linear T_s dependence [4, 6]. Assuming that $T_s/T_0 \simeq 1$, which will generally be true for micrometer-sized particles in atmospheric-pressure combustors, the distribution function for the reflected molecules can be expanded in a Taylor series about the ambient temperature T_0. By performing this expansion, and taking into account conservation of mass at the particle surface, the T_s dependence in the analysis can be linearized. Under this approximation, the net energy transfer from the surface can be written as [17]

$$-k_s \frac{\delta T_s}{\delta r} = \alpha \rho_g (2RT_0)^{3/2} \frac{T_s - T_0}{2\sqrt{\pi T_0}}, \quad r = a. \quad (33)$$

In non-dimensional form, equation (33) is expressed as

$$-\frac{\delta \bar{T}}{\delta \zeta} = H_m \bar{T}, \quad \zeta = 1 \quad (34)$$

where

$$H_m = \frac{4\alpha}{15}\frac{k_g}{k_s}\frac{a}{l}. \quad (35)$$

Using equation (34) as a boundary condition in the expression for $\bar{T}$, equation (9), the coefficients A_n are obtained as

$$A_n = \frac{G_n'(1) + H_m G_n(1)}{n + H_m}. \quad (36)$$

The surface temperature distribution is thus given by

$$\bar{T}(1,\mu) = \sum_{n=0}^{\infty} [G_n'(1) - nG_n(1)] \frac{P_n(\mu)}{n+H_m}. \quad (37)$$

In the linearized approximation, the net force from molecular momentum transfer acting upon a differential area element of the sphere is [17]

$$\frac{dF_z}{dA} = \frac{\alpha \rho_g R T_0}{4} \bar{T}(1,\mu)\cos\theta. \tag{38}$$

As was the case for the slip-flow problem, only the $n = 1$ term in equation (37) remains following integration of equation (38) over the particle surface. Consequently, the photophoretic force in the free molecular regime is given as

$$F_p = -\frac{\pi^2 \alpha \eta^2 I_\lambda a J_1}{6\rho_g k_s T_0} \frac{(a/l)^2}{1+H_m}. \tag{39}$$

For radiation absorbed entirely on the particle surface (i.e. $J_1 = -0.5 Q_{abs}$), the above expression for F_p will reduce exactly to that developed by Hidy and Brock [3].

Equating F_p to the expression for the particle drag, equation (31), the photophoretic velocity is

$$V_p = -\frac{\pi \alpha \eta I_\lambda a J_1}{36\rho_g k_s T_0} \frac{(a/l)^2[1+l/a(C_1+C_2 e^{-C_3 a/l})]}{1+H_m}. \tag{40}$$

In the free molecular limit, where $Kn \gg 1$, equation (40) reduces to

$$V_p(a/l \to 0) = -\frac{0.14 \alpha \eta I_\lambda a J_1}{\rho_g k_s T_0 l}. \tag{41}$$

5. EVALUATION OF THE PHOTOPHORETIC ASYMMETRY FACTOR J_1

Both the slip-flow (equation (32)) and the FML (equation (41)) expressions for V_p have the same dependency upon radiative absorption, which is embodied in the photophoretic asymmetry factor J_1 as given in equation (30). This parameter, which represents a weighted integration of the source function over the particle volume, was first identified by Yalamov *et al.* [8].

The internal heat generation is related to the internal electric field by equation (2). Using the formalism of Bohren and Huffman [20], the spherical components of the internal electric field for a plane incident wave of unit amplitude are given as

$$E_r = -\frac{\cos\psi}{m^2\rho^2} \sum_{n=1}^{\infty} i^{n+1}(2n+1) d_n \psi_n(m\rho) P_n^{(1)}(\mu) \tag{42}$$

$$E_\theta = \frac{\cos\psi}{m\rho} \sum_{n=1}^{\infty} i^n E_n (c_n \psi_n(m\rho)\pi_n(\mu) - i d_n \psi_n'(m\rho)\tau_n(\mu)) \tag{43}$$

$$E_\psi = -\frac{\sin\psi}{m\rho} \sum_{n=1}^{\infty} i^n E_n (c_n \psi_n(m\rho)\tau_n(\mu) - i d_n \psi_n'(m\rho)\pi_n(\mu)). \tag{44}$$

In the above, $\rho = 2\pi r/\lambda$ is the dimensionless radiative radial coordinate

$$E_n = (2n+1)/n(n+1)$$

ψ_n the Ricatti–Bessel function of order n and the prime denotes differentiation with respect to the argument. The functions π_n and τ_n are given by

$$\pi_n = \frac{P_n^{(1)}(\mu)}{\sin\theta} \tag{45}$$

$$\tau_n = \frac{d}{d\theta} P_n^{(1)}. \tag{46}$$

The coefficients c_n and d_n are

$$c_n = \frac{m\psi_n(x)\xi_n'(x) - m\psi_n'(x)\xi_n(x)}{\psi_n(mx)\xi_n'(x) - m\psi_n'(mx)\xi_n(x)} \tag{47}$$

$$d_n = \frac{m\psi_n(x)\xi_n'(x) - m\psi_n'(x)\xi_n(x)}{m\psi_n(mx)\xi_n'(x) - \psi_n'(mx)\xi_n(x)} \tag{48}$$

where $\xi_n = \psi_n + i\chi_n$ is the Ricatti–Bessel function of the third kind. For unpolarized incident radiation, the field components are obtained by setting $\psi = \pi/4$ [21]. It should also be noted that the refractive index is defined here as $m = n + i\kappa$.

Pluchino [10] evaluated J_1 through numerical quadrature of equation (30) using the above expressions. Considering that the number of significant terms in equations (42)–(44) is generally larger than the size parameter x, such computations can involve a considerable amount of time for large x. It was observed by Greene *et al.* [21] that the ability to determine accurately J_1 is contingent upon evaluation of the Ricatti–Bessel functions with a high degree of precision. Approximate analytical solutions for J_1 have been developed from geometrical optics [8] and Rayleigh-limit [16] considerations. In the following, it is demonstrated that equation (30) can be analytically integrated to yield a closed-form solution for J_1 applicable for arbitrary x and m.

Substitution of equations (42)–(44) into equation (2) yields the following terms:

$$E_r \cdot E_r^* = \frac{i}{2|m|^4\rho^4} \sum_{n=1}^{\infty}\sum_{l=1}^{\infty} i^{n+l+2}(-1)^{l+1} \times (2n+1)(2l+1) d_n d_l^* \psi_n \psi_l^* P_n^{(1)} P_l^{(1)} \tag{49}$$

$$E_\theta \cdot E_\theta^* + E_\phi \cdot E_\phi^* = \frac{1}{2|m|^2\rho^2} \sum_{n=1}^{\infty}\sum_{l=1}^{\infty} i^{n+l}(-1)^l E_n E_l \times ((c_n c_l^* \psi_n \psi_l^* + d_n d_l^* \psi_n' \psi_l'^*)(\pi_n \pi_l + \tau_n \tau_l) + i(c_n d_l^* \psi_n \psi_l'^* - d_n c_l^* \psi_n' \psi_l^*)(\pi_n \tau_l + \tau_n \pi_l)). \tag{50}$$

It should be realized in the above that the argument of ψ_n is $m\rho$ and that of τ_n and π_n is μ. In integration over μ, the following integral relationships can be derived [20]:

$$\int_{-1}^{1} (\tau_n \tau_l + \pi_n \pi_l)\mu \, d\mu = \frac{2n(n+1)^2(n-1)^2}{(2n+1)(2n-1)}, \quad |n-l| = 1, \quad n = \max(n,l)$$
$$= 0, \quad |n-l| \neq 1 \tag{51}$$

$$\int_{-1}^{1} (\tau_n \pi_l + \pi_n \tau_l)\mu \, d\mu = \frac{2n(n+1)}{2n+1}\delta(n-l) \tag{52}$$

$$\int_{-1}^{1} P_n^{(1)} P_l^{(1)} \mu \, d\mu = \frac{2n(n+1)(n-1)}{(2n+1)(2n-1)}, \quad |n-l| = 1,$$

$$n = \max(n, l)$$

$$= 0, \quad |n-l| \neq 1. \tag{53}$$

Multiplying equations (49) and (50) by $\mu \, d\mu$ and integrating from -1 to 1 yields

$$\int_{-1}^{1} E_r \cdot E_r^* \mu \, d\mu = \frac{-2}{|m|^4 \rho^4} \operatorname{Im} \sum_{n=1}^{\infty} n(n+1)(n+2) \times d_{n+1} d_n^* \psi_{n+1} \psi_n^* \tag{54}$$

$$\int_{-1}^{1} (E_\theta \cdot E_\theta^* + E_\phi \cdot E_\phi^*) \mu \, d\mu = \frac{-2}{|m|^2 \rho^2} \operatorname{Im} \sum_{n=1}^{\infty} \left(\frac{n(n+2)}{n+1} (c_{n+1} c_n^* \psi_{n+1} \psi_n^* + d_{n+1} d_n^* \psi'_{n+1} \psi_n'^*) - \frac{(2n+1)}{n(n+1)} d_n c_n^* \psi'_n \psi_n^* \right). \tag{55}$$

Utilizing the recurrence relationships for ψ_n, the above equations can be put in a form more amenable for integration over ρ. The following relationships are utilized:

$$\psi'_{n+1}(m\rho) \psi_n'^*(m\rho) = \psi_n \psi_n'^* - \frac{(n+1)^2}{|m|^2 \rho^2} \psi_{n+1} \psi_n^* + \frac{n+1}{m\rho} \psi_{n+1} \psi_{n+1}^* \tag{56}$$

$$\psi_{n+1}(m\rho) \psi_n^*(m\rho) = \frac{n+1}{m\rho} \psi_n \psi_n^* - \psi'_n \psi_n^*. \tag{57}$$

When these expressions are substituted into equation (55) and summed with equation (54), all $1/\rho^4$ terms cancel. As a result, one is left with

$$\int_{-1}^{1} \mathbf{E} \cdot \mathbf{E}^* \mu \, d\mu = \frac{-2}{|m|^2 \rho^2} \operatorname{Im} \sum_{n=1}^{\infty} \left(\frac{n(n+2)}{m\rho} (c_{n+1} c_n^* |\psi_n|^2 + d_{n+1} d_n^* |\psi_{n+1}|^2) - \left(\frac{n(n+2)}{n+1} (c_{n+1} c_n^* + d_n d_{n+1}^*) + \frac{2n+1}{n(n+1)} d_n c_n^* \right) \psi'_n \psi_n^* \right). \tag{58}$$

Equation (58) is now multiplied by $\rho^3 \, d\rho$ and integrated from 0 to x. The terms involving $|\psi_n(m\rho)|^2$ and $|\psi_{n+1}(m\rho)|^2$ can be integrated directly to yield

$$R_n \equiv \int_0^x |\psi_n(m\rho)|^2 \, d\rho = \frac{\operatorname{Im}[m \psi_{n+1}(mx) \psi_n^*(mx)]}{\operatorname{Im}(m^2)}. \tag{59}$$

The term involving $\psi'_n(m\rho) \psi_n^*(m\rho)$ can be integrated through use of the recurrence relations and consideration of real and imaginary parts. Denoting

$$S_n \equiv \int_0^x \rho \psi_n^*(m\rho) \psi'_n(m\rho) \, d\rho \tag{60}$$

the following expression can be derived:

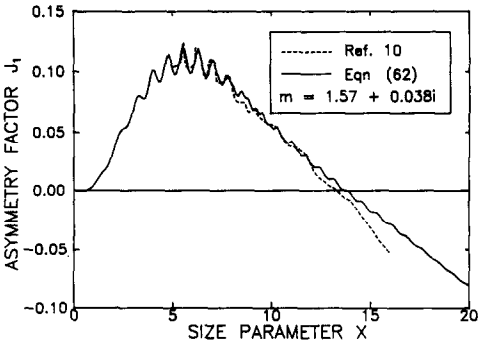

FIG. 1. Photophoretic asymmetry factor J_1 vs size parameter x. Results of ref. [10] and equation (62).

$$S_n = -\frac{-i}{2 \operatorname{Im}(m^2)} \left\{ x(m|\psi_n(mx)|^2 + m^* |\psi_{n+1}(mx)|^2) - \left(m + 2(n+1) \frac{\operatorname{Re}(m^2)}{m} \right) R_n + (2n+1) m^* R_{n+1} \right\}. \tag{61}$$

The expression for the photophoretic asymmetry factor J_1 can now be written as

$$J_1 = \frac{-6n\kappa}{|m|^2 x^3} \operatorname{Im} \sum_{n=1}^{\infty} \left(\frac{n(n+2)}{m} (c_{n+1} c_n^* R_n + d_{n+1} d_n^* R_{n+1}) - \left(\frac{n(n+2)}{n+1} (c_{n+1} c_n^* + d_n d_{n+1}^*) + \frac{2n+1}{n(n+1)} d_n c_n^* \right) S_n \right). \tag{62}$$

Numerical evaluation of equation (62) is discussed in the appendix.

Under certain situations, limiting behavior can be identified for J_1. For $x \gg 1$ and $k \gg 1$, corresponding to a large, highly absorbing sphere, all radiant energy is absorbed at or near the particle surface. Consequently, J_1 will approach the surface-absorption limiting value of $-0.5 Q_{abs}$. For the case where $x \gg 1$ and both $(n-1)$ and $kx \ll 1$, J_1 can be obtained explicitly from geometrical optics considerations, yielding [8]

$$J_1 = 2n\kappa x \left(\frac{3(n-1)}{8n^2} - \frac{2}{5} n\kappa x \right). \tag{63}$$

Evaluation of J_1 using equation (62) correctly obeyed the above limiting behavior.

The calculations of J_1 performed by Pluchino [10] appear to be the only published values to date, and comparison is made between these values and those obtained from equation (62) in Figs. 1 and 2. The curves present J_1 as a function of x for $m = 1.57 + 0.038i$ and $1.57 + 0.38i$, respectively. The 400 points used to generate the curves corresponding to equation (62), for size parameters from 0.05 to 20, required about 2 min of calculation on a 80287-based personal computer. The agreement is quite good, although in Fig. 1, J_1 obtained from equation (62) is slightly larger than the values of ref. [10] for x greater than around 14. Without additional information it is

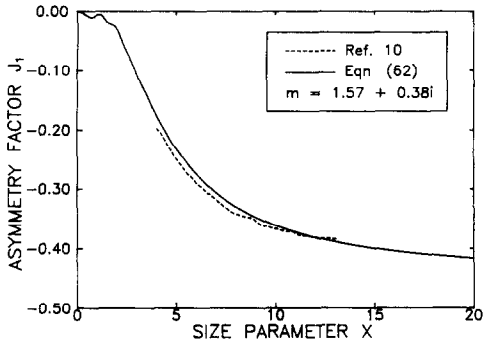

FIG. 2. Photophoretic asymmetry factor J_1 vs size parameter x. Results of ref. [10] and equation (62).

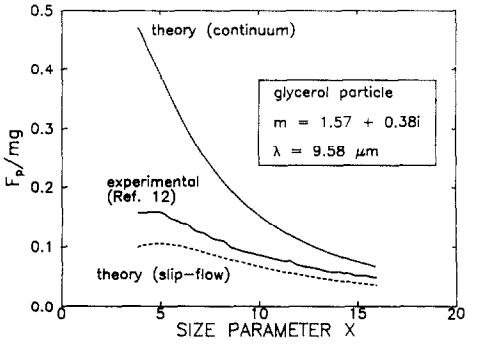

FIG. 4. Photophoretic force–particle weight ratio F_p/mg vs x. Results of experiment [12], slip-flow and continuum theories.

impossible to verify completely the calculations of equation (62). However, in view of the fact that the large majority of terms in $|\mathbf{E}|^2$, when integrated over $\mu\,d\mu$, are identically zero (i.e. equations (51)–(53)), numerical integration of equation (30) will likely produce significant error unless a high order of quadrature is utilized.

6. PHOTOPHORETIC FORCE RESULTS

There is not an abundance of accurate experimental measurements of the photophoretic force, although the photophoretic spectroscopy technique (PPS) recently developed by Arnold *et al.* [22] appears to be capable of providing a large amount of information on the photophoretic properties of aerosol particles. Their technique basically involves the levitation of a charged particle in a modified Millikan apparatus. Incident illumination upon the particle is provided with either a laser or a continuum source. By varying the wavelength of the continuum source, or, for the case of a volatile particle, allowing the particle to evaporate, the photophoretic force acting upon the particle can be obtained as a function of the particle size parameter.

Using the PPS technique, Arnold and Lewittes [12] obtained values of F_p/mg, where mg is the particle weight, for an evaporating glycerol particle. Measurements were made at two wavelengths (10.63 and 9.58 μm) at which the refractive indices of glycerol were estimated to be that given in Figs. 1 and 2, respectively. Figures 3 and 4 give the experimental F_p/mg results

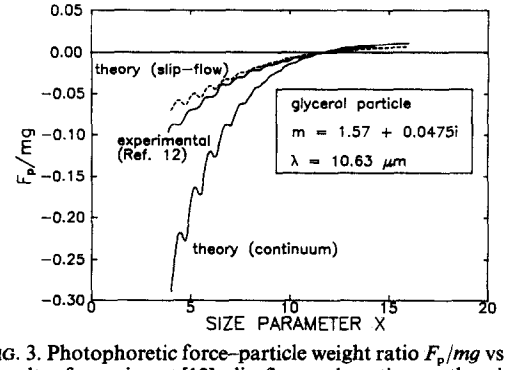

FIG. 3. Photophoretic force–particle weight ratio F_p/mg vs x. Results of experiment [12], slip-flow and continuum theories.

of ref. [8] and theoretical continuum- and slip-flow predictions obtained from equations (29) and (62). In Fig. 3, where the wavelength is 10.63 μm, the refractive index has been adjusted to $1.57+0.0475i$ so the calculated and measured reversal points (the transition from negative to positive photophoresis) coincide. In Fig. 4, for 9.58 μm, the refractive index is $1.57+0.38i$. Note that the magnitude of the slip-flow results are closer to the experimental values that the continuum-flow results. In addition, the ratio between the calculated and measured F_p/mg values are more nearly a constant for the slip- than the continuum-flow analysis. This indicates that the functional dependence of F_p on particle size and prevailing Knudsen number is correctly predicted by equation (29). As noted by Pluchino [10], the error between the calculated and measured curves is to be expected considering the difficulty in estimating the intensity of the incident beam falling upon the particle.

The free molecular limit photophoretic force analysis, given by equation (39), is now compared to the theory of Ahktaruzzaman and Lin [5] as calculated by Kerker and Cooke [11]. Presented in Fig. 5 are results of F_p calculated using the parameters given in ref. [11], which correspond to a pressure of 0.1 atm, $k_s = 5.0$ W m^{-1} K^{-1}, $\lambda = 0.6$ μm, and an incident intensity equal to the solar constant, 1353 W m^{-2}. When compared to the results of ref. [11], it is seen that the functional dependence of F_p is quite similar between the two theories, although some of the oscil-

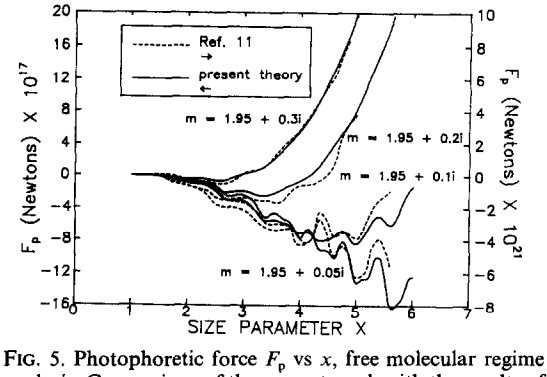

FIG. 5. Photophoretic force F_p vs x, free molecular regime analysis. Comparison of the present work with the results of ref. [11].

lations evident in the results of ref. [11] are damped out in the present analysis. Of concern is that F_p calculated from equation (39) is almost exactly 2×10^4 times greater than that presented in ref. [11]. The latter results are suspect, in that the authors state that their calculated F_p, which from their figures is of the order of 10^{-21} N, will, for a particle having a density of 1000 kg m^{-3} and a radius of around 0.35 μm, correspond to roughly 2–4% of the particle weight. Such a particle would actually weigh 1.8×10^{-15} N, so it is believed that the authors made an error in presenting their results. However, their conclusion regarding the photophoretic force relative to the particle weight is consistent with the results of the present analysis.

A significantly larger photophoretic force was predicted from the Monte-Carlo numerical calculations of Sitarski and Kerker [6]. For gas and particulate properties similar to those presented in Fig. 5, the authors indicate that the photophoretic force on submicrometer aerosol particles exposed to solar radiation can exceed the particle weight. This result is at odds with the present analysis. The value of J_1 yielding a photophoretic force, for the above conditions, equal to the particle weight would be well in excess of unity. From physical considerations, the maximum value of J_1 would occur if the radiant energy within the particle was absorbed entirely within an infinitesimal volume furthest from the source of radiation, i.e. at the point $r = a$ and $\theta = 0$. Using a delta-function representation of $Q(r, \mu)$, it can be shown that this situation would result in $J_1 = 0.75 Q_{abs}$. As the absorption efficiency Q_{abs} is typically less than 2 or 3 [20], the results obtained in ref. [6] appear to be physically unrealistic. The confirmation (or rejection) of the theoretical predictions, however, will have to wait until accurate experimental measurements of F_p in the free molecular limit become available.

7. PHOTOPHORESIS IN COMBUSTION ENVIRONMENTS

The analyses for the photophoretic velocity V_p given in Sections 3 and 4 considered the case of a plane, monochromatic incident radiation beam. Such conditions are obviously not realistic in combustion environments. A complete analysis of the photophoretic behavior of particles in, say, PC furnaces, would have to account for the directional and spectral distribution of the incident radiation as well as the spectral dependence of the particle refractive index m.

In order to provide initial estimates of the importance of photophoresis as a particulate transport mechanism, some assumptions are made concerning the directional and spectral dependencies. First of all, it is assumed that the spectral intensity I_λ appearing in equations (32) and (40) can be replaced with the radiative heat flux $q_{R\lambda}$. Secondly, the radiation source can be characterized by an effective radiation temperature T_R and wavelength-independent emittance ε such that

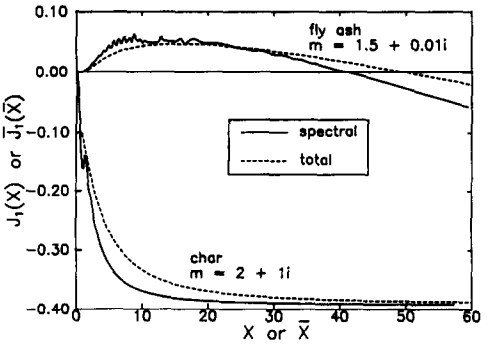

FIG. 6. Spectral and total asymmetry factor. Char and fly ash particles.

$$q_{R\lambda} = \varepsilon e_{b\lambda}(T_R) \tag{64}$$

where $e_{b\lambda}(T_R)$ is the Planck blackbody function. Thirdly, the refractive index of the particle is assumed constant.

For the above conditions, a wavelength-integrated, or total, photophoretic asymmetry factor J_1 can be defined by

$$\bar{J}_1 = \frac{1}{\sigma T_R^4} \int_0^\infty J_1(x, m) e_{b\lambda}(T_R)\, d\lambda. \tag{65}$$

By defining a 'thermal radiation size parameter' $\bar{x} = 2\pi a T_R/(\lambda T)_{max}$, where $(\lambda T)_{max} = 2898$ μm K corresponds to the Wein displacement law, $\bar{J}_1$ can be expressed as a function of $\bar{x}$ and m.

Curves of spectral $J_1(x)$ and total $\bar{J}_1(\bar{x})$ are presented in Fig. 6. The two values of refractive index used in generating the curves were chosen to roughly correspond to char particles ($m = 2 + 1i$) and fly ash ($m = 1.5 + 0.01i$) [23]. As can be seen from Fig. 6, the differences in m between char and fly ash can result in significantly different photophoretic behavior. The highly-absorbing char particles will experience a positive photophoresis (in the radiation direction) for all x or $\bar{x}$, whereas the relatively low-absorbing fly ash undergoes negative photophoresis up to a value of $\bar{x}$ of around 50. The total $\bar{J}_1$ curves are seen to be shifted somewhat to the right of the spectral J_1 curves, and the oscillations evident in J_1 for fly ash at small x are damped out in the corresponding $\bar{J}_1$. Comparison of the spectral and integrated curves indicate that the 'effective' wavelength of blackbody radiation, for estimation of $\bar{J}_1$ from $J_1(x)$, is around $\lambda = 0.8(\lambda T)_{max}/T_R$.

For particulate-deposition oriented research, it is convenient to define a 'photophoretic diffusivity' analogous to the thermophoretic diffusivity $\alpha_T D$, where α_T is the thermophoretic diffusivity factor and D the particle Brownian diffusion coefficient [1], such that

$$V_p = \alpha_p D \frac{q_R}{k_g T_0}. \tag{66}$$

For atmospheric pressure furnaces, the mean-free-path of the gas molecules and the effective wavelength of radiation will be of the order of 0.1 and 1 μm, respectively. Considering that J_1 rapidly goes to zero

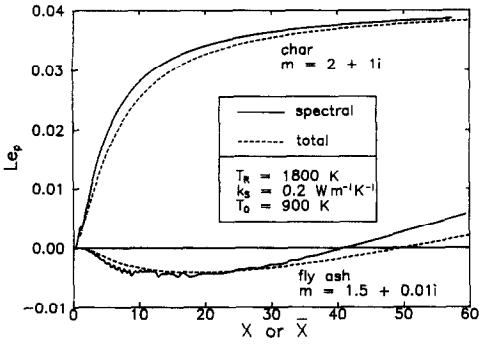

FIG. 7. Photophoretic Lewis number Le_p vs x. Char and fly ash particles.

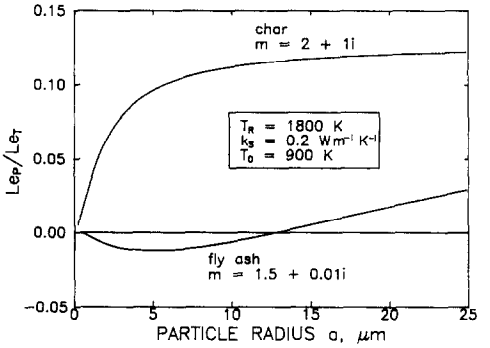

FIG. 8. Ratio of photophoretic and thermophoretic Lewis numbers Le_p/Le_T vs particle radius. Char and fly ash particles.

for $x < 1$, the effect of photophoresis on free molecular limit particles will be negligible in such furnaces when compared to other transport mechanisms, e.g. thermophoresis. Consequently, $\alpha_p D$ is more usefully defined using the slip-flow expression for V_p. The appropriate non-dimensional form of the photophoretic diffusivity is the ratio between this quantity and the thermal diffusivity of the gas, which can be considered a Lewis number for photophoresis. Using equation (32), the photophoretic Lewis number Le_p is

$$Le_p = \frac{V_p \rho_g c_p T_0}{q_R} = \frac{2\eta c_s c_p \bar{J}_1}{3k_s} \times \frac{1 + l/a(C_1 + C_2 e^{-C_3 a/l})}{(1 + 3c_m l/a)(1 + 2c_t l/a + 2k_g/k_s)}. \quad (67)$$

Presented in Fig. 7 are curves for Le_p for char and fly ash particles, in which T_0 and k_s were taken as 900 K and 0.2 W m^{-1} K^{-1}, respectively, and air was taken as the host gas. For size parameters greater than around 5, the magnitude of Le_p is of the order of 0.01. Photophoretic velocities calculated for typical PC furnace conditions [23] will generally be of the order of 1–5 cm s^{-1}.

It is known that thermophoresis plays a major role in the deposition of submicrometer to slightly supermicrometer combustion particulates [1, 14]. For larger particle radii, inertial impaction becomes dominant. It is therefore of interest to examine the ratio $Le_p/Le_T = (V_p/q_R)/(V_T/q_c)$, where V_T is the thermophoretic velocity and q_c the local conductive (Fourier) heat flux. Using the slip-flow expression for V_T developed by Brock [17, 18], this ratio is

$$\frac{Le_p}{Le_T} = \frac{\bar{J}_1 k_g}{3k_s(k_g/k_s + c_t l/a)}. \quad (68)$$

An interesting physical interpretation of $\bar{J}_1$ is provided by the above result, in that $\bar{J}_1$ can be seen as three times the continuum-limit ratio of the photophoretic and thermophoretic velocities for equal radiative and conductive heat flux.

Curves of Le_p/Le_T are presented in Fig. 8 as a function of particle radius for an assumed radiation temperature $T_R = 1800$ K. For a 2 μm radius, this ratio is around -0.008 for fly ash and 0.10 for char particles. Considering that radiative heat fluxes in PC furnaces can be of the order of 20 times greater than conductive fluxes, the clear implication of Fig. 8 is that, for slightly supermicrometer particles, photophoresis can be a significant mode of particulate transport and deposition. The current efforts are aimed at providing a more detailed analysis of the role of photophoresis in combustion environments.

Acknowledgements—It is a pleasure to acknowledge the DOE-PETC (Grant No. DE-FG22-86PC90756) and the Yale HTCRE Laboratory Industrial Affiliates (Shell, ACVO-Lycoming, SCM-Chemicals) for the financial support which made this research possible. The author is indebted to Prof. D. E. Rosner for motivating this evaluation of the role of particle photophoresis in combustion engineering applications, and, in particular, for suggesting the dimensionless photophoretic 'diffusivity' presentation included in Section 7.

REFERENCES

1. D. E. Rosner, *Transport Processes in Chemically Reacting Flow Systems*, Chap. 8. Butterworths, Stoneham, Massachusetts (1986); 2nd Edn (1988).
2. S. A. Varma, *Pulverized Coal Combustion and Gasification* (Edited by L. D. Smoot and D. T. Pratt), p. 311. Plenum Press, New York (1979).
3. G. M. Hidy and J. R. Brock, Photophoresis and the descent of particles in the lower atmosphere, *J. Geophys. Res.* **72**, 455–460 (1967).
4. N. T. Tong, Photophoretic force in the free molecule and transition regimes, *J. Colloid Interface Sci.* **43**, 78–84 (1973).
5. A. F. M. Ahktaruzzaman and S. P. Lin, Photophoresis of absorbing particles, *J. Colloid Interface Sci.* **61**, 171–182 (1977).
6. M. Sitarski and M. Kerker, Monte Carlo simulation of photophoresis of submicron aerosol particles, *J. Atmos. Sci.* **41**, 2250–2262 (1984).
7. L. D. Reed, Low Knudsen number photophoresis, *J. Aerosol Sci.* **8**, 123–131 (1977).
8. Yu. I. Yalamov, V. B. Kutukov and E. R. Shchukin, Theory of the photophoretic motion of the large-size volatile aerosol particle, *J. Colloid Interface Sci.* **57**, 564–571 (1976).
9. P. W. Dusel, M. Kerker and D. D. Cooke, Distribution of absorption centers within irradiated spheres, *J. Opt. Soc. Am.* **69**, 55–59 (1979).
10. A. B. Pluchino, Photophoretic force on particles for low Knudsen number, *Appl. Opt.* **22**, 103–106 (1983).
11. M. Kerker and D. D. Cooke, Photophoretic force on

aerosol particles in the free-molecule regime, *J. Opt. Soc. Am.* **72,** 1267–1272 (1982).
12. S. Arnold and M. Lewittes, Size dependence of the photophoretic force, *J. Appl. Phys.* **53,** 5314–5319 (1982).
13. N. A. Fuchs, *The Mechanics of Aerosols*, p. 62. Pergamon Press, New York (1964).
14. D. E. Rosner and J. Fernandez de la Mora, Small particle transport across turbulent nonisothermal boundary layers, *J. Engng Pwr* **104,** 885–894 (1982).
15. S.-W. Kang, A. F. Sarofim and J. M. Beer, Particle rotation in coal–water fuel combustion: statistical, experimental and theoretical studies, Twenty-second (International) Symposium on Combustion, Seattle, Washington (1988).
16. S. Arnold, A. B. Pluchino and K. M. Leung, Influence of surface-mode-enhanced local fields on photophoresis, *Phys. Rev. A.* **29,** 654–660 (1984).
17. L. Talbot, R. K. Cheng, R. W. Schefer and D. R. Willis, Thermophoresis of particles in a heated boundary layer, *J. Fluid Mech.* **101,** 737–758 (1980).
18. J. R. Brock, On the theory of thermal forces acting on aerosol particles, *J. Colloid Sci.* **17,** 768–780 (1962).
19. L. D. Landau and E. M. Lifshitz, *Fluid Mechanics*, p. 63. Pergamon Press, Oxford (1959).
20. C. F. Bohren and D. R. Huffman, *Absorption and Scattering of Light by Small Particles*, Chap. 4. Wiley, New York (1983).
21. W. M. Greene, R. E. Spjut, E. Bar-Ziv, A. F. Sarofim and J. P. Longwell, Photophoresis of irradiated spheres: absorption centers, *J. Opt. Soc. Am. B.* **2,** 998–1004 (1985).
22. S. Arnold, Y. Amani and A. Orenstein, Photophoretic spectrometer, *Rev. Scient. Instrum.* **51,** 1202–1204 (1980).
23. R. Viskanta and M. P. Menguc, Radiation heat transfer in combustion systems, *Prog. Energy Combust. Sci.* **13,** 97–160 (1987).

APPENDIX. NUMERICAL EVALUATION OF J_1

Computation of J_1 via equation (62) was accomplished through a slight modification of the BHMIE code given in ref. [20]. BHMIE is an efficient FORTRAN program for calculation of extinction and scattering properties of a homogeneous sphere.

In order to utilize BHMIE for the present purpose, equation (62) is reformulated using the logarithmic derivative function $D_n = \psi_n'(mx)/\psi_n(mx)$. This can be accomplished by dividing equation (62) through by $|\psi_n(mx)|^2$, which yields the following terms:

$$\bar{R}_n \equiv \frac{R_n}{|\psi_n(mx)|^2} = \frac{\mathrm{Im}\,(mC_n)}{\mathrm{Im}\,(m^2)} \tag{A1}$$

$$\bar{S}_n \equiv \frac{S_n}{|\psi_n(mx)|^2} = -\frac{-\mathrm{i}}{2\,\mathrm{Im}\,(m^2)}\left\{x(m+m^*|C_n|^2) - \left(m+2(n+1)\frac{\mathrm{Re}\,(m^2)}{m}\right)\bar{R}_n + (2n+1)m^*|C_n|^2\bar{R}_{n+1}\right\} \tag{A2}$$

where

$$C_n \equiv \frac{\psi_{n+1}(mx)}{\psi_n(mx)} = \frac{n+1}{mx} - D_n. \tag{A3}$$

The internal wave coefficients c_n and d_n are related to the BHMIE-calculated scattered wave coefficients a_n and b_n by

$$\bar{c}_n \equiv \psi_n(mx)c_n = m[\psi_n(x) - \xi_n(x)b_n] \tag{A4}$$

$$\bar{d}_n \equiv \psi_n(mx)d_n = \psi_n(x) - \xi_n(x)a_n. \tag{A5}$$

Substituting equations (A1)–(A5) into equation (62) yields

$$J_1 = \frac{-6n\kappa}{|m|^2x^3}\,\mathrm{Im}\sum_{n=1}^{\infty}\left(\frac{n(n+2)}{m}\left(\frac{\bar{c}_{n+1}\bar{c}_n^*\bar{R}_n}{C_n} + \bar{d}_{n+1}\bar{d}_n^*\bar{R}_{n+1}C_n^*\right) - \left(\frac{n(n+2)}{n+1}\left(\frac{\bar{c}_{n+1}\bar{c}_n^*}{C_n} + \frac{\bar{d}_n\bar{d}_{n+1}^*}{C_n^*}\right) + \frac{2n+1}{n(n+1)}\bar{d}_n\bar{c}_n^*\right)\bar{S}_n\right). \tag{A6}$$

The advantage of using the function $D_n(mx)$ as opposed to $\psi_n(mx)$ is that the former is much easier to calculate for arbitrary orders of n [20]. Calculations of J_1 using equation (A5) were found to agree with the results of equation (62) in which $\psi_n(mx)$ was evaluated explicitly from a series expansion.

PHOTOPHORESE DES PARTICULES D'AEROSOL DANS LES REGIMES MOLECULAIRES LIBRES ET DE GLISSEMENT

Résumé—On présente une analyse de la force photophorétique et des particules d'aérosol dans le régime moléculaire libre et celui du glissement. Avec les hypothèses d'un rayonnement incident non polarisé, l'absorption du rayonnement dans la particule est formulée à partir de la théorie de Lorentz/Mie. Pour les régimes moléculaires libres et ceux de glissement, la dépendance fonctionnelle de la vitesse photophorétique vis-à-vis du paramètre de dimension et de l'indice complexe de réfraction est donné par le facteur J_1 d'assymétrie photophorétique. Une expression en série infinie de J_1 est obtenue pour calculer rapidement le comportement photophorétique. Des résultats numériques montrent que la photophorèse peut être un mécanisme de transport significatif pour les particules microscopiques dans les environnements en combustion avec des transferts radiatifs intenses.

PHOTOPHORESE VON AEROSOL-TEILCHEN IM BEREICH GROSSER UND KLEINER FREIER WEGLÄNGEN

Zusammenfassung—Es wird eine Untersuchung der photophoretischen Kraft und Geschwindigkeit an Aerosol-Teilchen im Bereich großer und kleiner ("slip-flow") freier Weglängen vorgestellt. Unter der Annahme, daß unpolarisierte Strahlung einfällt, wurde mittels der Theorie von Lorenz/Mie die Absorption von Strahlung im Partikel beschrieben. Für beide Bereiche (große und kleine freie Weglänge) gibt der photophoretische Asymmetriefaktor J_1 die Abhängigkeit der photophoretischen Geschwindigkeit vom Strahlungsparameter und vom komplexen Brechungsindex an. J_1 wird in eine genaue unendliche Reihe entwickelt, die eine schnelle Berechnung des photophoretischen Verhaltens erlaubt. Numerische Ergebnisse zeigen, daß die Photophorese ein bedeutender Transportmechanismus für Partikel der Größenordnung "mikro-meter" in hochbelasteten Strahlungsbrennkammern sein kann.

ФОТОФОРЕЗ АЭРОЗОЛЬНЫХ ЧАСТИЦ ПРИ СВОБОДНОМОЛЕКУЛЯРНОМ РЕЖИМЕ И РЕЖИМЕ ТЕЧЕНИЯ СО СКОЛЬЖЕНИЕМ

Аннотация—В предположении неполяризованности падающего излучения на основе теории Лоренца/Мии определено поглощение излучения частицей. Для обоих режимов свободномолекулящного течения и течения со скольжением при помощи асимметричного коэффициента фотофореза J_1 найдена функциональная зависимость скорости фотофореза от параметра излучения и комплексного коэффициента преломления. Получено точное выражение для J_1 в виде бесконечного ряда, позволяющее быстро определять характер фотофореза. Численные результаты показывают, что фотофорез может служить важным механизмом переноса частиц микронного размера в сильно излучающих средах при горении.